Anti-MUC1-C Antibody–Conjugated Nanoparticles Potentiate the Efficacy of Fractionated Radiation Therapy

Alexandre Detappe, Clélia Mathieu, Caining Jin, Michael P. Agius, Marie-Charlotte Deringer, Vu-Long Tran, Xavier Pivot, François Lux, Olivier Tillement, Donald Kufe, et al.

Anti-MUC1-C Antibody-conjugated Nanoparticles Potentiate the Efficacy of Fractionated Radiation Therapy

Short-running title (46 characters): Anti-MUC1-C/NP radiotherapy enhancer

Detappe A, Ph.D.*[1,2], Mathieu C, M.Sc.[1], Jin C, Ph.D.[1], Agius M, Ph.D.[1], Diringer MC, M.Sc.[2], Tran VL, Ph.D.[3], Pivot X, M.D., Ph.D.[4], Lux F, Ph.D.[3,5], Tillement O, Ph.D.[3], Kufe D, M.D.*[1], and Ghoroghchian PP, M.D., Ph.D.*[1]

1. Dana-Farber Cancer Institute, Department of Medical Oncology, Harvard Medical School, 02215, Boston MA, USA
2. Centre Paul Strauss, 67000 Strasbourg, France
3. Institut Lumière-Matière, UMR 5306, Université Lyon1-CNRS, Université de Lyon, 69622 Villeurbanne Cedex, France
4. Institut du Cancer Strasbourg, 67000 Strasbourg, France
5. Institut Universitaire de France

*To whom correspondence should be addressed:

Alexandre Detappe, Ph.D.
Centre Paul Strauss
3 Porte de l'Hôpital
67000 Strasbourg
email : a.detappe@icans.eu

Donald Kufe, M.D.
Dana-Farber Cancer Institute
450 Brookline Avenue
Boston, MA 02215
email: Donald_Kufe@DFCI.HARVARD.EDU

P. Peter Ghoroghchian, M.D., Ph.D.
Dana-Farber Cancer Institute
450 Brookline Avenue
Boston MA 02215
email: Paiman_Ghoroghchian@DFCI.HARVARD.EDU

Funding statement: A.D. acknowledges support from the Philippe Foundation. Research reported in this publication was supported by the National Cancer Institute of the National Institutes of Health under grant numbers CA97098, CA166480, CA229716 and CA233084 awarded to D.W.K. P.P.G. acknowledges support from the Charles W. and Jennifer C. Johnson Clinical Investigator Fund and from the Kathryn Fox Samway Foundation.

Conflict of interest: F.L. and O.T. are employees from NH TherAguix, Inc. F.L., O.T., and A.D. are shareholders of NH Theraguix, Inc., which holds the patent rights to the AGuIX® NPs described in this publication.

Statistical analysis was performed by AD (a.detappe@icans.eu).

All data generated and analyzed during this study are included in this published article (and its supplementary information files). Raw data can be requested to by joining the corresponding authors.

Abstract

Purpose: Heavy-metal chelators and inorganic nanoparticles (NPs) have been examined as potential radioenhancers to increase the efficacy of external beam radiation therapy of various cancers. Most of these agents have, unfortunately, displayed relatively poor pharmacokinetic properties, which limit the percentages of injected dose (%ID/g) that localize to tumors and which shorten the window for effective radiation enhancement due to rapid tumor washout.

Materials and Methods: To address these challenges, we sought to conjugate gadolinium-based ultra-small (<5 nm) NPs to an antibody directed against the oncogenic MUC1-C subunit that is overexpressed on the surfaces of many different human cancer types. Note that the binding of the anti-MUC1-C antibody 3D1 to MUC1-C on the surface of a cancer cell is associated with its internalization and, thereby, to effective intracellular delivery of the antibody-associated payload, promoting its effective tumor retention. As such, we examined whether systemically administered anti-MUC1-C antibody-conjugated, gadolinium-based NPs (anti-MUC1-C/NPs) could accumulate within cell-line xenograft models of MUC1-C-expressing (H460) lung and (E0771) breast cancers to improve the efficacy of radiation therapy (XRT).

Results: The %ID/g of anti-MUC1-C/NPs that accumulated within tumors was found to be similar to that of their unconjugated counterparts (6.6 ± 1.4 vs. 5.9 ± 1.7 %ID/g, respectively). Importantly, the anti-MUC1-C/NPs demonstrated prolonged retention in *in vivo* tumor microenvironments; and, as a result, the radiation boost was maintained over the course of fractionated therapy (3 x 5.2 Gy). We found that by administering anti-MUC1-C/NPs with XRT, it was possible to significantly augment tumor growth inhibition and to prolong the animals' overall survival (46.2 ± 3.1 days) when compared to the administration of control NPs with XRT (31.1 ± 2.4 days) or with XRT alone (27.3 ± 1.6 days; $p < 0.01$, log-rank).

Conclusion: These findings suggest that anti-MUC1-C/NPs could be employed to enhance the effectiveness of radiation therapy and potentially to improve clinical outcomes.

Introduction

Gold nanoparticles (NPs) were the first NP-based radioenhancers to be tested in small animals for tumor therapy[1, 2]. Their ability to augment the efficacy of external bean radiation was found to be mediated via the photoelectric effect and by Auger electron showers that arise due to the interactions between gold atoms and low energy photons produced by the external beam[3-5]. Based on these early findings, various inorganic NPs have been subsequently developed to similarly boost the efficacy of radiation therapy[6], including ones comprised of bismuth, hafnium,[7-9] and gadolinium,[10-13] amongst others[14, 15]. Simulation studies conducted by McMahon and colleagues demonstrated that localized dose escalation is directly linked to the amount of internalized NP per cell and not to the atomic number of the metal comprising the NP[16]. Since this seminal report, various approaches have been adopted to improve the internalization of radioenhancers in preclinical tumor models, including through functionalization of NPs with antibodies[17, 18] to aide in tumor targeting.[18, 19] Efforts have also focused upon optimization of the timing of radiation via imaging of the same NP construct by computed tomography (CT)[20, 21] or by magnetic resonance imaging (MRI).[11, 12]

The aforementioned preclinical studies have provided the rationale for clinical trials based on 2 separate NP compositions and via 2 distinct routes of administration. Hafnium oxide-based NPs (NBTXR3) injected intratumorally in a hydrogel have been imaged effectively by CT, demonstrating persistence inside the tumor bed post-implantation as well as limited diffusion outside of the injection site[8, 9]. In parallel, gadolinium-containing NPs (AGuIX) that were administered intravenously (IV) have been successfully tracked by MRI, enabling radiation therapy only after tumor localization[10, 22]. Both studies have demonstrated promising results and support the generalized capabilities of inorganic NPs to serve as radioenhancers in

clinical applications. While IV injection of imaging agents enables accessibility to a multitude of cancers, NPs administered via the IV route have been shown to rapidly wash out from tumors if not internalized by tumor cells as was observed in the NANO-RAD trial (NCT02820454). In that study, the gadolinium-based NPs were injected once weekly over the course of radiation therapy. After a single administration, the NPs initially localized within tumor environments but were then rapidly washed out, which was a phenomenon that could be attributed to their accumulation in perivascular spaces and their inability to specifically bind or to be taken up by tumor cells. The observed tumor wash out likely underlies their inability to enhance radiation over the full course of therapy and highlights the necessity for repeated NP administration to maintain early radiation boost effects.

Given these findings, we hypothesized that NPs that are engineered to persist within the tumor environment could more effectively enhance the dose of fractionated radiation treatment and could obviate the need for repeated radioenhancer administration, which could decrease potential morbidities and/or treatment-related costs. In the present study, we conjugated multiple NPs to a single tumor-specific monoclonal antibody (mAb) to increase the dose of radioenhancer that is delivered to tumor cells. As the target for these antibody-conjugated NPs, we selected mucin 1 (MUC1) based on its high expression levels across a variety of solid and hematologic malignancies[23]. MUC1 consists of an extracellular subunit (MUC1-N) and a transmembrane subunit (MUC1-C). Effective antibody-based targeting of MUC1-N has proven elusive due to its continuous shedding from the tumor cell surface[24, 25]. In contrast, the transmembrane MUC1-C subunit, which is not shed, functions as a potent oncoprotein, driving an aggressive tumor phenotype[26]. We have recently demonstrated targeting of the MUC1-C extracellular domain with the mAb 3D1[27]. 3D1 binds to a conserved alpha3 helix that is not expressed in other proteins and selectivity reacts with malignant cells across a variety of cancer types. In order to compare the radioenhancement properties of 3D1-conjugated NPs (i.e., anti-MUC1-C/NPs) to their unconjugated counterparts, we utilized the same type of nanoparticles that were employed in the NANO-RAD trial[28] (**Fig.S1**); both

compositions were administered in combination with either a single high dose of external beam or with fractionated radiation therapy; and, treatment effects were compared in various models of lung and triple-negative breast cancer (**Fig. 1A**).

Results and Discussion

Synthesis of gadolinium-containing ultra-small nanoparticles. NPs were synthesized by following a previously established protocol[28] that incorporates the silane precursors tetraethyl orthosilicate (TEOS) and aminopropyl triethoxysilane (APTES) with the macrocyclic chelator DOTAGA anhydride (1,4,7,10-tetraazacyclododecane-1-glutaric anhydre-4,7,10-triacetic acid) in a one-pot synthesis; the resultant APTES-DOTAGA conjugates are then complexed with Gd^{3+}, using a solution of $GdCl_3$. Thereafter, they are isolated and mixed with other organic silanes to generate the NPs (**Fig. 1B**, **Fig. S1**). The advantages of NPs produced by this method, versus those constructed by a bottoms-up approach that is typically employed to synthesize other gadolinium-based NPs for clinical applications, are the facility afforded by swapping and comparing the activities of various metallic atoms that can be complexed with different chelators in order to control physical properties through reproducible experimental conditions. With an average hydrodynamic diameter of 6.3 ± 1.7 nm (as determined via dynamic light scatting; DLS) and a favorable stability profile (as examined over 3 days in solution; **Fig. S2**), these ultra-small gadolinium-based NPs were found to be comparable to those examined previously in the NANO-RAD trial, *vide supra*, and were advanced for further anti-MUC1-C mAb conjugation.

Conjugation of nanoparticles to anti-MUC1-C antibodies. Modification of the free amino groups of 3D1 with transcyclooctene (TCO) enabled coupling to tetrazine (Tz) groups present on the surfaces of NPs[29] via established click chemistry protocols (**Fig. 1C**). TCO binding to Tz was validated by MALDI-MS (**Fig. S3**) and was optimized by using model reactions that examined various ratios of PEG_4-TCO to Tz-modified antibody. Bulk UV-VIS measurements were utilized to follow modification of NPs, wherein the change in ABS of Tz

at 517 nm was correlated to TCO-Tz coupling over time (**Fig. S4**). These experiments demonstrated that 33.6 TCO per anti-MUC1-C 3D1 mAb provided for optimal conjugation. Lower amounts of TCO did not result in sufficiently high levels of NP conjugation, yielding no detectable levels of fluorescently-labeled NPs after incubation with MUC1-C+ E0771 (murine triple negative breast cancer[30]) cells in culture; similarly, higher amounts of TCO per mAb did not result in better binding (**Fig. S3**). The final composition of the resultant anti-MUC1-C/NPs was determined by ICP-MS after removal of excess unreacted reagent, using a tangential filtration device equipped with a 15 nm size cutoff and by following previously published protocols[31]. These experiments determined that 4.1 ± 1.8 NPs bound to a single 3D1 mAb, which was consistent with a previously study[31].

To examine the capabilities of the anti-MUC1-C/NPs to bind tumor cells, we labeled the NPs with Cy5.5 prior to mAb coupling and confirmed their specific uptake by MUC1-C+ human E0771 breast cancer cells via fluorescence microscopy (**Fig. 1D**). The presence of the Cy5.5 dye also enabled confirmation of cellular labeling with anti-MUC1-C/NPs via flow cytometry, which was conducted after NP incubation with (i) MUC1-C+ E0771 cells (**Fig. 1E**) and (ii) MUC1-C+ human H460 lung cancer cells[32] before and after silencing of MUC1-C expression, using a lentiviral vector encoding a MUC1-C shRNA[33] (**Fig. S5**). For both cell lines, >95% cellular-labeling with Cy5.5 was observed only after incubation with Cy5.5-conjugated anti-MUC1-C/NPs as compared to various controls. The specificity of MUC1-C binding by the Cy5.5-conjugated anti-MUC1-C/NPs was further confirmed in a blocking experiment wherein pre-incubation of the same cells with free and unlabeled anti-MUC1-C mAb (i.e, 3D1) was conducted prior to addition of the labeled NPs, yielding <15% cellular labeling with the fluorophore and confirming the binding specificity of anti-MUC1-C/NPs.

***In vitro* studies of radiation enhancement.** The radioenhancement properties of the anti-MUC1-C/NPs were examined using the E0771 and H460 cancer cell lines prior to advancing to animal studies. Clonogenic assays were performed after irradiating cells with 0 to 10 Gy

doses, which were delivered in a single fraction by the small animal radiation research platform (SARRP). Augmentation of radiation-induced inhibition of *in vitro* cellular expansion was observed for cells treated with either unconjugated NPs or anti-MUC1-C/NPs as compared to those treated with radiation alone ($p = 0.019$, and $p = 0.014$, Mann Whitney test, respectively). The sensitive enhancement ratio (SER) values, which are defined as the radiation dose needed to reach a survival fraction of 50% in the radiation-containing treatment groups without and with the addition of radioenhancers[34], were similar for anti-MUC1-C/NPs and their unconjugated (free NP) counterparts, equaling 1.69 (vs. 1.32) and 1.86 (vs. 2.00) in E0771 and in H460 cells, respectively. These SER values are also similar to those obtained with AGuIX NPs as reported with various cell lines[35], which confirmed a macroscopic radiation boost increase of approximately 25%. Note that there were no differences observed between the passive (NP) and the actively targeted (anti-MUC1-C/NP) groups ($p = 0.42$, Mann Whitney test) (**Fig. 2A**). The local dose enhancement was further confirmed by a DNA-damage assay based on staining for γH2AX foci at 15 min after exposure to a 2 Gy dose of radiation (**Fig. 2B**). Quantification of the number of γH2AX foci (**Fig. 2C**), which can be directly correlated to the numbers of double-stranded DNA breaks within the genome of cells, confirmed a significant increase observed with both XRT + nanoparticle-containing treatment groups (XRT + NP and XRT + anti-MUC1-C/NP groups) in comparison to the XRT only group (*i.e.*, $p = 0.021$ and $p = 0.027$, Mann-Whitney test, respectively).

In vivo applications. A preliminary evaluation of the *in vivo* pharmacology of anti-MUC1-C/NPs was conducted in healthy Balb/c mice. Animals were injected intravenously with nanoparticles (350 mg/kg of Gd^{3+} in 0.2 mL PBS) alone or after conjugation to anti-MUC1-C mAb (i.e., anti-MUC1-C/NPs). The circulatory persistence of the anti-MUC1-C/NPs was found to be enhanced when compared to that of unconjugated NPs, demonstrating a half-life of 28.6 vs. 16.8 min, respectively (**Fig. S6**). At 72 h post-administration of either formulation, only traces amounts of Gd^{3+} were detected in the liver, lungs, or other major organs of

treated mice as quantitively determined via inductively-coupled plasma mass spectrometry (ICP-MS) (**Fig. S7**). These findings are consistent with those of previous studies with the base nanoparticle formulation (NPs) upon conjugation to an mAb against the B cell maturation antigen (BCMA) and when examined in preclinical models of multiple myeloma[31]. In the current study, histologic examination of H&E stained tissues sections was performed by a veterinary pathologist upon necroscopy at 20 days after treatment administration and demonstrated no overt signs of acute tissue toxicities (**Fig. S8**), which was similarly consistent with the previous study[31].

Based on these encouraging findings, we conducted further experiments to evaluate the potential utility of our NP constructs to serve as radioenhancers for cancer therapy. We employed two distinct murine models: (i) a subcutaneous xenograft model of lung cancer that was generated via implantation of human H460 lung cancer cells in the flanks of Balb/c nude mice; and, (ii) an orthotopic and syngeneic model of triple negative breast cancer that was generated by implantation of E0771 cells in the mammary fat pads of B6(Cg)-Tyrc-2J/J mice. In order to determine the optimal window for radiation enhancement, which is defined as the time period whereby the maximal treatment effect is observed for the first irradiation fraction while avoiding concomitant toxicities to healthy surrounding tissues, the biodistribution patterns of fluorescently-labeled NPs and anti-MUC1-C/NPs were examined via *in vivo* optical imaging, using the orthotopic triple-negative breast cancer model. Imaging was conducted at various time points after IV administration of each formulation (**Fig. 3A**); at time points >1 h post-injection, negligible signals were observed in the heart, lungs, and healthy breast tissues of the treated mice. This time period after administration further allowed for substantial uptake of the nanoparticles within the tumor bed (6.6 ± 1.4%ID/g at 1 h, 4.3 ± 1.1%ID/g at 24 h, 3.8 ± 0.9%ID/g at 48 h), which was sufficient to generate a significant radiation boost. At 24 h post injection, residual NPs that were neither internalized nor surface-associated through MUC1-C-binding to tumor cells were observed to clear from the tumor microenvironment (**Fig. 3B**). Note that at this dose and (IV) mode of administration, no

treatment group (i.e., unconjugated NPs, anti-IgG/NPs, nor anti-MUC1-C/NPs) whether alone or in combination with XRT was found to promote overt healthy-tissue toxicities as determined by serial body-weight measurements in the orthotopic (E0771) breast tumor model (**Fig. 3C**).

We hypothesized that the prolonged tumor retention characteristics exhibited by anti-MUC1-C/NPs could potentially obviate the practice of employing multiple injections to provide radiation enhancement, which has previously been deemed necessary when utilizing untargeted NPs to impart treatment effects[10, 36]. To test this possibility, we first employed a single fraction of high-dose stereotaxic radiation (10 Gy), which was administered in concert with different nanoparticle and control formulations. Irradiation was performed with a 220 kVp X-ray beam (SARRP platform), whereby 2 orthogonal beams were used to uniformly treat the entire tumor of each animal (**Fig. S9**)[12]. Using the subcutaneous (H460) lung cancer model (n=5 mice/group), we compared the radiation enhancement properties of anti-MUC1-C/NPs to those of the untargeted nanoparticle formulations (i.e., unconjugated NPs and anti-IgG/NPs) that were administered at the same total dose (350 mg/kg of Gd^{3+}) (**Fig. 4A**). Based on the preliminary pharmacology experiments, *vide supra*, all nanoparticle and control (PBS) groups were administered via a single IV (tail-vein) injection at 1 h prior to irradiation in order to provide sufficient time for their accumulation within tumor environments. After animal irradiation, tumor sizes and body weights were monitored twice per week. For each subject, the study was terminated once its tumor reached size > 3 cm in any axis or when it experienced a >20% loss in body weight. Compared to mice in the control group (i.e., PBS + XRT alone) that lived for 26.4 ± 3.2 days, animals that were similarly administered radiation in conjugation with any nanoparticle formulation demonstrated significant improvements in tumor growth delay ($p = 0.033$, Mann Whitney test) as well as a prolongation in survival (to 29.3 ± 2.1 days in the unconjugated NP, 30.1 ± 1.6 days in the anti-IgG/NP, and 30.3 ± 1.6 days in the anti-MUC1-C/NP groups; $p<0.001$, Log-Rank test). Note that when administered

in combination with a single fraction of high-dose radiation, there were no differences in survival imparted between any NP-containing treatment groups ($p>0.05$, Log-Rank test).

To investigate the potential for anti-MUC1-C/NPs to impart preferential enhancements in combination with fractionated radiation treatment (3x5.2Gy), a second therapeutic study was conducted whereby radiation was delivered at 1, 24, and 48 h after anti-MUC1-C/NPs, untargeted NPs (i.e., unconjugated NPs or anti-IgG/NPs), or after control (PBS) administration and by using the same dosimetry approach. Note that the total radiation dose in this study was equivalent to the single 10 Gy that was administered in the first study, *vide supra*, as based on the linear quadratic model equation. We hypothesized that with fractionated - as opposed to single high-dose – administration, the radiation boost to the tumor bed could be maximized for subjects in the anti-MUC1-C/NP group due to their enhanced persistence that was imparted by specific surface binding and/or internalization by tumor cells. By again employing the subcutaneous (H460) lung tumor model, we observed significant enhancements in tumor growth delay ($p= 0.024$, Mann-Whitney test) and in overall survival ($p<0.001$, Log-Rank test) for animals in the anti-MUC1-C/NP group (median survival of 46.2 ± 3.1 days) when compared to mice treated with either untargeted NPs (median survival of 31.1 ± 2.4 and 29.1 ± 2.2 days with unconjugated NPs and with anti-IgG/NPs, respectively) or with control (PBS + XRT) administration (median survival of 27.3 ± 1.6 days; **Fig. 4B)**.

Given the potential confounder of enhanced tumor vascularity, and thereby nanoparticle delivery, that may be exhibited by subcutaneous xenotransplanted tumors in murine model systems[37], we sought to further employ the orthotopic and syngeneic (E0771) breast tumor model to validate the putative radioenhancement properties imparted by combining anti-MUC1-C/NPs with fractionated XRT and in comparison to untargeted NPs and (PBS) control. E0771 cells that are implanted in the mammary fat pad have previously been shown to recapitulate the same vascular, metastatic and treatment resistance patterns of human triple-

negative breast cancer[38]. Irradiation, which was conducted by using 2 orthogonal beams and which focused upon the mammary fat pad of the animal, was performed at 1, 24, and 48 h after (IV) administration of each treatment group. The same endpoints were adopted as with the previous therapeutic study (in the subcutaneous model, *vide supra)*; and, the results were consistent between the two model systems, demonstrating significant improvements in overall survival for mice that received fractionated radiation in combination with any NP-containing treatment group and when compared to those that received radiation or the same NP treatments alone (**Fig. 4C**). The greatest effects where seen with animals that received fractionated radiation therapy in conjunction with anti-MUC1-C/NPs, exhibiting a >15-day improvement in overall survival when compared to all other groups. Upon reaching the study endpoint, the tumor from each mouse was extracted and its histologic features were examined after H&E staining (**Fig. 4D**). Large fractions of necrosis (28.8 ± 5.4%) were observed in the tumors of animals that were treated with both fractionated radiation and anti-MUC1-C/NPs, confirming the observed radiation boost when compared with the animals that were treated with XRT+NP (7.6 ± 3.2 % necrosis, $p<0.01$, Mann Whitney test) or with XRT alone (3.5 ± 1.9% necrosis, $p<0.001$, Mann Whitney test)

Conclusions

Upon systemic administration of untargeted NPs, a small fraction accrues in the perivascular spaces of tumors, wherein constructs that are comprised of heavy metals may be used as radioenhancers to augment treatment effects. Over time, the majority of these extravasated NPs are cleared from tumor environments via the lymphatics, by reentry into the systemic circulation and/or via non-specific internalization by select tumor and stromal cells. Here, we demonstrate that ultra-small Gd^{3+}-containing NPs that are conjugated to an anti-MUC1-C antibody exhibit prolonged retention in both subcutaneous and orthotopically-implanted tumors in murine model systems, thereby improving radioenhancement properties when combined with fractionated radiation therapy. Such augmentation in properties suggest that

these anti-MUC1-C/NPs may afford for less frequent and/or smaller total dose administrations to achieve comparable effectiveness to that observed with their untargeted NP counterparts. If validated in future translational studies, our exemplified method may be utilized with other antibody-targeted NPs, rendering a potentially powerful approach for radiation enhancement that is generalizable and mediated entirely by antibody specificity. The applications of such constructs may further translate into lower costs, reduced radiation doses, improved safety profiles, and/or improved clinical outcomes for patients.

Material and Methods

Anti-MUC1-C monoclonal antibody: Dry aliquots of the anti-MUC1-C mAb 3D1 were freshly prepared by dissolution in PBS (5 mL) and thereafter stored at 4 ºC prior to use.

Synthesis of NP formulations: To a freshly prepared solution of APTES-DOTAGA (11.7 mM, pH 4) was added $GdCl_3$ in 3 equal aliquots to a final molar ratio of APTES–DOTAGA:Gd of 1:0.9; the solution pH was thereafter monitored and maintained. Upon 48 h of incubation at 80 °C, the solution was adjusted to pH 9; TEOS (2 eq) and APTES (1 eq) were added; and, the volume of water was adjusted to obtain final concentrations of APTES-DOTAGA(Gd^{3+}), APTES-DOTAGA, TEOS and APTES of 9, 1, 20, and 10 mM, respectively. This mixture was subsequently stirred for an additional 18 h at 25 °C, adjusted to pH 4.5, and further incubated for 18 h at 80 °C to generate the NP suspensions. The solution pH was then adjusted to 2; and, NPs were concentrated and purified by tangential ultrafiltration, using the Vivaspin® device (MWCO = 3 kDa; SigmaAldrich). The NP suspension was further filtered through a 0.2 mm membrane (SigmaAldrich) and freeze-dried for longer-term storage. NP compositions were characterized by DLS and by HPLC analyses. Prior to biological application, they were resuspended with Gd^{3+} (10 mM). To generate fluorophore-labelled NP constructs, small volume additions (0.1 mL) of a stock solution of Cy5.5-NHS ester (10 mM in DMSO) were added to NPs slowly and under agitation to a final molar ratio of 1:500 Cy5.5 to Gd^{3+} in solution. For antibody coupling, NPs were further surface modified upon small volume additions (1 mL) of a stock solution of Tz-PEG_4-NHS ester (10 mM in DMSO) and to a final molar ratio of 1:10 Tz to Gd^{3+}. All modified NP suspensions were then stirred for 5 h at RT and thereafter purified by tangential ultracentrifugation, using the Vivaspin® device (MWCO = 3 kDa). The number of Tz groups in Tz-PEG_4-NP suspensions were determined by UV-vis spectroscopy. The complexes were then purified by using a tangential filtration device equipped with a 50 kDa molecular weight cutoff membrane (Millipore) as previously

described[31]. The final concentrations of the anti-MUC1-C/NPs were determined by ICP-MS, using an Agilent 7900 instrument (Agilent Technologies, Inc.).

Clonogenic assay: Various NP-based treatment groups (0.4 mg/mL of Gd^{3+}) were incubated with E0771 and H460 cells for 45 min prior to cellular irradiation with a dose of 2, 4, 6, 8, or 10 Gy, which was administered with a 220 kVp X-ray beam (SARRP, Xstrahl). Following previously reported protocols,[39, 40] the treated cells were subsequently incubated for 6 h, thereafter counted, re-seeded in 10 cm dishes (at 300 cells per plate), and allowed to grow for an additional 10 d before staining with a dye solution comprised of 1% crystal violet in 10% ethanol; foci were then counted manually.

Quantification of DNA damage: Various NP-based treatment groups (0.4 mg/mL of Gd^{3+}) were incubated with E0771 for 30 min prior to irradiation with 2 Gy. The treated cells were then fixed with 4% paraformaldehyde in PBS for 30 min at RT. Fixed cells were blocked with 1% BSA, 10% FBS, and 0.3% tritonX-100 in PBS prior to staining overnight at 4°C with anti-γH2AX antibody (Millipore). Following previously reported protocols,[39, 40] a secondary anti-mouse AlexaFluor-594 conjugated IgG (Abcam) was used for staining and micrographs were obtained by using an upright Carl Zeiss microscope with an HXP 120C light source and a 63x/1.4 oil plan-apochromat objective. Semiquantitative analyses were conducted to compare the numbers of foci per cell expressing γH2Ax. The signal intensities of individual foci were quantified by using the CellProfiler cell imaging software (version 3.1.8).

Animal experiments: All animals experiments were performed in accordance with the rules and regulations set-forth by the IACUC of the hospital and under an approved protocol (#03-029).

Toxicity studies: Healthy female Balb/c nude mice were injected (IV) with a single dose of either PBS, NP, NP-IgG, anti-MUC1-C mAb (3D1), or anti-MUC1-C/NPs. Their body weights

were monitored daily, starting on the day of injection. Blood was collected by submandibular puncture to determine the half-life of the different NP formulations. After 20 days, the major organs of the animals were collected and stained with H&E prior to histological analyses by a board-certified veterinary pathologist..

Biodistribution study: 5-week old female B6(Cg)-Tyrc-2J/J mice were implanted with E0771 cells (1 million via mammary fat pad injection). They were included in study when their tumors reached >7 mm in largest axis and were administered one of the following treatments (n = 5 mice/group per timepoint): PBS (control), unmodified NPs, or anti-MUC1-C/NPs (350 mg/kg of Gd^{3+}; 5 mg/kg of anti-MUC1-C mAb). Cy5.5-bound NPs were tracked by imaging after IV administration, using an IVIS Spectrum-bioluminescence and fluorescence imaging system (Perkins Elmer) for qualitative quantification. ICP-MS measurements were performed to confirm the presence of NPs in the major organs at different timepoints after IV administration, following previously established protocols[31].

Therapeutic studies: 5-week old female Balb/c nude mice were implanted with H460 cells (1 million cells under the skin) and B6(Cg)-Tyrc-2J/J mice were implanted with E0771 cells (1 million cells via mammary fat pad injection) to establish the subcutaneous (lung) and orthotopic (triple negative breast) tumor models, respectively. Animals were included in the study when their tumors reached >7 mm in largest axis and were administered one of the following treatments (n = 5 mice/group): PBS (control), unmodified NPs, or anti-MUC1-C/NPs (350 mg/kg of Gd^{3+}; 5 mg/kg of anti-MUC1-C) alone or in further combination with external beam radiation (*vide infra*); untargeted (i.e., anti-IgG) NPs administered at the same dose and in combination with XRT served as an additional control. Mice were administered a single dose of each NP group by IV tail-vein injection at 30 min prior to irradiation with either a single dose of 10 Gy or with 3 equal fractions of 5.2 Gy each, which were delivered with a 220 kVp X-ray beam collimated to the tumor size and by using the SARRP platform[12]. Tumor sizes were thereafter monitored daily by using calipers; and, animals were removed from

study when their tumor reached >3 cm in the largest axis, when they exhibited >15% loss in body weight or when they were moribund.

References

1. Hainfeld, J. F.; Slatkin, D. N.; Smilowitz, H. M., The use of gold nanoparticles to enhance radiotherapy in mice. *Phys Med Biol* **2004,** *49* (18), N309-15.

2. Schuemann, J.; Berbeco, R.; Chithrani, D. B.; Cho, S. H.; Kumar, R.; McMahon, S. J.; Sridhar, S.; Krishnan, S., Roadmap to Clinical Use of Gold Nanoparticles for Radiation Sensitization. *Int J Radiat Oncol Biol Phys* **2016,** *94* (1), 189-205.

3. Butterworth, K. T.; McMahon, S. J.; Currell, F. J.; Prise, K. M., Physical basis and biological mechanisms of gold nanoparticle radiosensitization. *Nanoscale* **2012,** *4* (16), 4830-8.

4. Berbeco, R. I.; Detappe, A.; Tsiamas, P.; Parsons, D.; Yewondwossen, M.; Robar, J., Low Z target switching to increase tumor endothelial cell dose enhancement during gold nanoparticle-aided radiation therapy. *Med Phys* **2016,** *43* (1), 436.

5. Detappe, A.; Tsiamas, P.; Ngwa, W.; Zygmanski, P.; Makrigiorgos, M.; Berbeco, R., The effect of flattening filter free delivery on endothelial dose enhancement with gold nanoparticles. *Med Phys* **2013,** *40* (3), 031706.

6. Liu, Y.; Zhang, P.; Li, F.; Jin, X.; Li, J.; Chen, W.; Li, Q., Metal-based NanoEnhancers for Future Radiotherapy: Radiosensitizing and Synergistic Effects on Tumor Cells. *Theranostics* **2018,** *8* (7), 1824-1849.

7. Chen, M. H.; Hanagata, N.; Ikoma, T.; Huang, J. Y.; Li, K. Y.; Lin, C. P.; Lin, F. H., Hafnium-doped hydroxyapatite nanoparticles with ionizing radiation for lung cancer treatment. *Acta Biomater* **2016,** *37*, 165-73.

8. Bonvalot, S.; Rutkowski, P. L.; Thariat, J.; Carrere, S.; Ducassou, A.; Sunyach, M. P.; Agoston, P.; Hong, A.; Mervoyer, A.; Rastrelli, M.; Moreno, V.; Li, R. K.; Tiangco, B.; Herraez, A. C.; Gronchi, A.; Mangel, L.; Sy-Ortin, T.; Hohenberger, P.; de Baere, T.; Le Cesne, A.; Helfre, S.; Saada-Bouzid, E.; Borkowska, A.; Anghel, R.; Co, A.; Gebhart, M.;

Kantor, G.; Montero, A.; Loong, H. H.; Verges, R.; Lapeire, L.; Dema, S.; Kacso, G.; Austen, L.; Moureau-Zabotto, L.; Servois, V.; Wardelmann, E.; Terrier, P.; Lazar, A. J.; Bovee, J.; Le Pechoux, C.; Papai, Z., NBTXR3, a first-in-class radioenhancer hafnium oxide nanoparticle, plus radiotherapy versus radiotherapy alone in patients with locally advanced soft-tissue sarcoma (Act.In.Sarc): a multicentre, phase 2-3, randomised, controlled trial. *Lancet Oncol* **2019,** *20* (8), 1148-1159.

9. Bonvalot, S.; Le Pechoux, C.; De Baere, T.; Kantor, G.; Buy, X.; Stoeckle, E.; Terrier, P.; Sargos, P.; Coindre, J. M.; Lassau, N.; Ait Sarkouh, R.; Dimitriu, M.; Borghi, E.; Levy, L.; Deutsch, E.; Soria, J. C., First-in-Human Study Testing a New Radioenhancer Using Nanoparticles (NBTXR3) Activated by Radiation Therapy in Patients with Locally Advanced Soft Tissue Sarcomas. *Clin Cancer Res* **2017,** *23* (4), 908-917.

10. Lux, F.; Tran, V. L.; Thomas, E.; Dufort, S.; Rossetti, F.; Martini, M.; Truillet, C.; Doussineau, T.; Bort, G.; Denat, F.; Boschetti, F.; Angelovski, G.; Detappe, A.; Cremillieux, Y.; Mignet, N.; Doan, B. T.; Larrat, B.; Meriaux, S.; Barbier, E.; Roux, S.; Fries, P.; Muller, A.; Abadjian, M. C.; Anderson, C.; Canet-Soulas, E.; Bouziotis, P.; Barberi-Heyob, M.; Frochot, C.; Verry, C.; Balosso, J.; Evans, M.; Sidi-Boumedine, J.; Janier, M.; Butterworth, K.; McMahon, S.; Prise, K.; Aloy, M. T.; Ardail, D.; Rodriguez-Lafrasse, C.; Porcel, E.; Lacombe, S.; Berbeco, R.; Allouch, A.; Perfettini, J. L.; Chargari, C.; Deutsch, E.; Le Duc, G.; Tillement, O., AGuIX((R)) from bench to bedside-Transfer of an ultrasmall theranostic gadolinium-based nanoparticle to clinical medicine. *Br J Radiol* **2018**, 20180365.

11. Detappe, A.; Kunjachan, S.; Drane, P.; Kotb, S.; Myronakis, M.; Biancur, D. E.; Ireland, T.; Wagar, M.; Lux, F.; Tillement, O.; Berbeco, R., Key clinical beam parameters for nanoparticle-mediated radiation dose amplification. *Sci Rep* **2016,** *6*, 34040.

12. XXX.

13. Du, F.; Zhang, L.; Zhang, L.; Zhang, M.; Gong, A.; Tan, Y.; Miao, J.; Gong, Y.; Sun, M.; Ju, H.; Wu, C.; Zou, S., Engineered gadolinium-doped carbon dots for magnetic resonance imaging-guided radiotherapy of tumors. *Biomaterials* **2017,** *121*, 109-120.

14. Hainfeld, J. F.; Ridwan, S. M.; Stanishevskiy, Y.; Panchal, R.; Slatkin, D. N.; Smilowitz, H. M., Iodine nanoparticles enhance radiotherapy of intracerebral human glioma in mice and increase efficacy of chemotherapy. *Sci Rep* **2019,** *9* (1), 4505.

15. Minafra, L.; Porcino, N.; Bravata, V.; Gaglio, D.; Bonanomi, M.; Amore, E.; Cammarata, F. P.; Russo, G.; Militello, C.; Savoca, G.; Baglio, M.; Abbate, B.; Iacoviello, G.; Evangelista, G.; Gilardi, M. C.; Bondi, M. L.; Forte, G. I., Radiosensitizing effect of curcumin-loaded lipid nanoparticles in breast cancer cells. *Sci Rep* **2019,** *9* (1), 11134.

16. McMahon, S. J.; Hyland, W. B.; Muir, M. F.; Coulter, J. A.; Jain, S.; Butterworth, K. T.; Schettino, G.; Dickson, G. R.; Hounsell, A. R.; O'Sullivan, J. M.; Prise, K. M.; Hirst, D. G.; Currell, F. J., Biological consequences of nanoscale energy deposition near irradiated heavy atom nanoparticles. *Sci Rep* **2011,** *1*, 18.

17. Chattopadhyay, N.; Fonge, H.; Cai, Z.; Scollard, D.; Lechtman, E.; Done, S. J.; Pignol, J. P.; Reilly, R. M., Role of antibody-mediated tumor targeting and route of administration in nanoparticle tumor accumulation in vivo. *Mol Pharm* **2012,** *9* (8), 2168-79.

18. Retif, P.; Pinel, S.; Toussaint, M.; Frochot, C.; Chouikrat, R.; Bastogne, T.; Barberi-Heyob, M., Nanoparticles for Radiation Therapy Enhancement: the Key Parameters. *Theranostics* **2015,** *5* (9), 1030-44.

19. Kunjachan, S.; Detappe, A.; Kumar, R.; Ireland, T.; Cameron, L.; Biancur, D. E.; Motto-Ros, V.; Sancey, L.; Sridhar, S.; Makrigiorgos, G. M.; Berbeco, R. I., Nanoparticle Mediated Tumor Vascular Disruption: A Novel Strategy in Radiation Therapy. *Nano Lett* **2015,** *15* (11), 7488-96.

20. Deng, J.; Xu, S.; Hu, W.; Xun, X.; Zheng, L.; Su, M., Tumor targeted, stealthy and degradable bismuth nanoparticles for enhanced X-ray radiation therapy of breast cancer. *Biomaterials* **2018,** *154*, 24-33.

21. Detappe, A.; Thomas, E.; Tibbitt, M. W.; Kunjachan, S.; Zavidij, O.; Parnandi, N.; Reznichenko, E.; Lux, F.; Tillement, O.; Berbeco, R., Ultrasmall Silica-Based Bismuth Gadolinium Nanoparticles for Dual Magnetic Resonance-Computed Tomography Image Guided Radiation Therapy. *Nano Lett* **2017,** *17* (3), 1733-1740.

22. Verry, C.; Sancey, L.; Dufort, S.; Le Duc, G.; Mendoza, C.; Lux, F.; Grand, S.; Arnaud, J.; Quesada, J. L.; Villa, J.; Tillement, O.; Balosso, J., Treatment of multiple brain metastases using gadolinium nanoparticles and radiotherapy: NANO-RAD, a phase I study protocol. *BMJ Open* **2019,** *9* (2), e023591.

23. Nath, S.; Mukherjee, P., MUC1: a multifaceted oncoprotein with a key role in cancer progression. *Trends Mol Med* **2014,** *20* (6), 332-42.

24. Kufe, D. W., Mucins in cancer: function, prognosis and therapy. *Nat Rev Cancer* **2009,** *9* (12), 874-85.

25. Kufe, D. W., Functional targeting of the MUC1 oncogene in human cancers. *Cancer Biol Ther* **2009,** *8* (13), 1197-203.

26. Kufe, D. W., MUC1-C oncoprotein as a target in breast cancer: activation of signaling pathways and therapeutic approaches. *Oncogene* **2013,** *32* (9), 1073-81.

27. XXX

28. XXX

29. Haun, J. B.; Devaraj, N. K.; Hilderbrand, S. A.; Lee, H.; Weissleder, R., Bioorthogonal chemistry amplifies nanoparticle binding and enhances the sensitivity of cell detection. *Nat Nanotechnol* **2010,** *5* (9), 660-5.

30. Domcke, S.; Sinha, R.; Levine, D. A.; Sander, C.; Schultz, N., Evaluating cell lines as tumour models by comparison of genomic profiles. *Nat Commun* **2013,** *4*, 2126.

31. XXX

32. Shames, D. S.; Wistuba, I. I., The evolving genomic classification of lung cancer. *J Pathol* **2014,** *232* (2), 121-33.

33. Kharbanda, A.; Rajabi, H.; Jin, C.; Alam, M.; Wong, K. K.; Kufe, D., MUC1-C confers EMT and KRAS independence in mutant KRAS lung cancer cells. *Oncotarget* **2014,** *5* (19), 8893-905.

34. Detappe, A.; Kunjachan, S.; Rottmann, J.; Robar, J.; Tsiamas, P.; Korideck, H.; Tillement, O.; Berbeco, R., AGuIX nanoparticles as a promising platform for image-guided radiation therapy. *Cancer Nanotechnol* **2015,** *6* (1), 4.

35. Sancey, L.; Lux, F.; Kotb, S.; Roux, S.; Dufort, S.; Bianchi, A.; Cremillieux, Y.; Fries, P.; Coll, J. L.; Rodriguez-Lafrasse, C.; Janier, M.; Dutreix, M.; Barberi-Heyob, M.; Boschetti, F.; Denat, F.; Louis, C.; Porcel, E.; Lacombe, S.; Le Duc, G.; Deutsch, E.; Perfettini, J. L.; Detappe, A.; Verry, C.; Berbeco, R.; Butterworth, K. T.; McMahon, S. J.; Prise, K. M.; Perriat, P.; Tillement, O., The use of theranostic gadolinium-based nanoprobes to improve radiotherapy efficacy. *Br J Radiol* **2014,** *87* (1041), 20140134.

36. Bort, G.; Lux, F.; Dufort, S.; Crémillieux, Y.; Verry, C.; Tillement, O., EPR-mediated tumor targeting using ultrasmall-hybrid nanoparticles: From animal to human with theranostic AGuIX nanoparticles. *Theranostics* **2020,** *10* (3), 1319-1331.

37. Hofmann, C. L.; O'Sullivan, M. C.; Detappe, A.; Yu, Y.; Yang, X.; Qi, W.; Landon, C. D.; Therien, M. J.; Dewhirst, M. W.; Ghoroghchian, P. P.; Palmer, G. M., NIR-emissive PEG-b-TCL micelles for breast tumor imaging and minimally invasive pharmacokinetic analysis. *Nanoscale* **2017,** *9* (36), 13465-13476.

38. Maeda, T.; Hiraki, M.; Jin, C.; Rajabi, H.; Tagde, A.; Alam, M.; Bouillez, A.; Hu, X.; Suzuki, Y.; Miyo, M.; Hata, T.; Hinohara, K.; Kufe, D., MUC1-C Induces PD-L1 and Immune Evasion in Triple-Negative Breast Cancer. *Cancer Res* **2018,** *78* (1), 205-215.

39. He, Y. J.; Meghani, K.; Caron, M. C.; Yang, C.; Ronato, D. A.; Bian, J.; Sharma, A.; Moore, J.; Niraj, J.; Detappe, A.; Doench, J. G.; Legube, G.; Root, D. E.; D'Andrea, A. D.; Drane, P.; De, S.; Konstantinopoulos, P. A.; Masson, J. Y.; Chowdhury, D., DYNLL1 binds to MRE11 to limit DNA end resection in BRCA1-deficient cells. *Nature* **2018,** *563* (7732), 522-526.

40. Drane, P.; Brault, M. E.; Cui, G.; Meghani, K.; Chaubey, S.; Detappe, A.; Parnandi, N.; He, Y.; Zheng, X. F.; Botuyan, M. V.; Kalousi, A.; Yewdell, W. T.; Munch, C.; Harper, J. W.; Chaudhuri, J.; Soutoglou, E.; Mer, G.; Chowdhury, D., TIRR regulates 53BP1 by masking its histone methyl-lysine binding function. *Nature* **2017,** *543* (7644), 211-216.

Figures

Figure 1. **Antibody-targeted nanoparticles for radiation sensitization**. A) Conjugation of transcyclootene (TZO)-functionalized anti-MUC1-C antibody (mAb) to tetrazine (Tz)-modified ultra-small gadolinium-containing nanoparticles (NPs) via trans–cyclooctene (TCO–Tz) chemistry, generating anti-MUC1-C/NPs. B) Schematic representation of the accumulation of anti-MUC1-C/NPs in tumors to augment radiation effects. C) Fluorescence microscopy of MUC1-C+ E0771 cells (nuclei stained with DAPI; blue) after incubation with Cy5.5-labeled anti-MUC1-C/NPs (red), demonstrating binding of the latter to the extracellular membrane of the cells. D) Flow cytometry of MUC1-C+ and MUC1-C- (i.e., MUC1-C-siRNA silenced) E0771 cells (control) after incubation with anti-MUC1-C/NPs alone or in combination with free (i.e., competing) anti-MUC1-C mAb and as compared to PBS (control), confirming the specificity imparted by the anti-MUC1-C mAb-conjugated NPs.

Figure 2. **Gadolinium-containing nanoparticles enhance the effects of radiation therapy on cultured tumor cell lines**. A) Clonogenic assay on H460 (lung) and E0771 (triple-negative breast) cancer cells treated with different doses of radiation alone (XRT) or in combination with either untargeted or anti-MUC1-C/NPs that were incubated with the cells for 3 h and at equivalent doses (0.5 mg/mL). B) Fluorescence imaging of γH2AX foci in micrographs of E0771 cells (dotted) that were incubated for 3 h with various treatment groups before (-XRT) and after radiation (+XRT) administration (2Gy). C) Quantification of the numbers of γH2AX foci (observed amongst 250 counted cells) for E0771 (top) and H460 cells (bottom) that were treated with various control or NP formulations either alone or in combination with radiation (2 Gy).

Figure 3. **Pharmacology, biodistribution and gross toxicity experiments with anti-MUC1-C/NPs**. **A**) *In vivo* optical imaging and **B**) quantitative biodistribution (via ICP-MS for Gd content in excised tissues) at various timepoints after the systemic administration of Cy5.5-labeled untargeted (i.e., NP and anti-IgG) NPs and antibody-conjugated (anti-MUC1-C) NPs in the orthotopic breast tumor model (i.e., E0771 cells implanted in the mammary fat pads of C57BL/6 mice); untargeted NPs demonstrated rapid tumor washout while the antibody-conjugated constructs were found to persist within tumor environments for > 48 h. **C**) Body weight measurements of breast tumor-bearing mice at various time points after a single administration of various treatment groups alone (control) or after either single high-dose (XRT (10 Gy)) or fractionated radiation therapy (XRT (3x5.2 Gy)).

Figure 4. **Potential therapeutic utility of combining anti-MUC1-C/NPs with radiation**. A) Tumor growth and Kaplan Meier survival curves for orthotopic breast-tumor bearing mice (i.e., B6(Cg)-Tyrc-2J/J mice with E0771 cells implanted in their mammary fat pads) that were administered various NP or control formulations alone or in combination with a single high dose of external beam radiation (10 Gy). Tumor growth and survival were followed in B) the subcutaneous (H460) lung tumor-bearing model and C) the orthotopic breast-tumor model as a function of administration of the same NP and control groups alone or in combination with fractionated radiation therapy (3x5.2 Gy). C) Representative images of H&E-stained tumor micrographs after the last day of RT (20 days after tumor implantation), confirming increased necrosis in a tumor from an animal that was administered anti-MUC1-C/NPs followed by fractionated radiation (3x5.2 Gy).

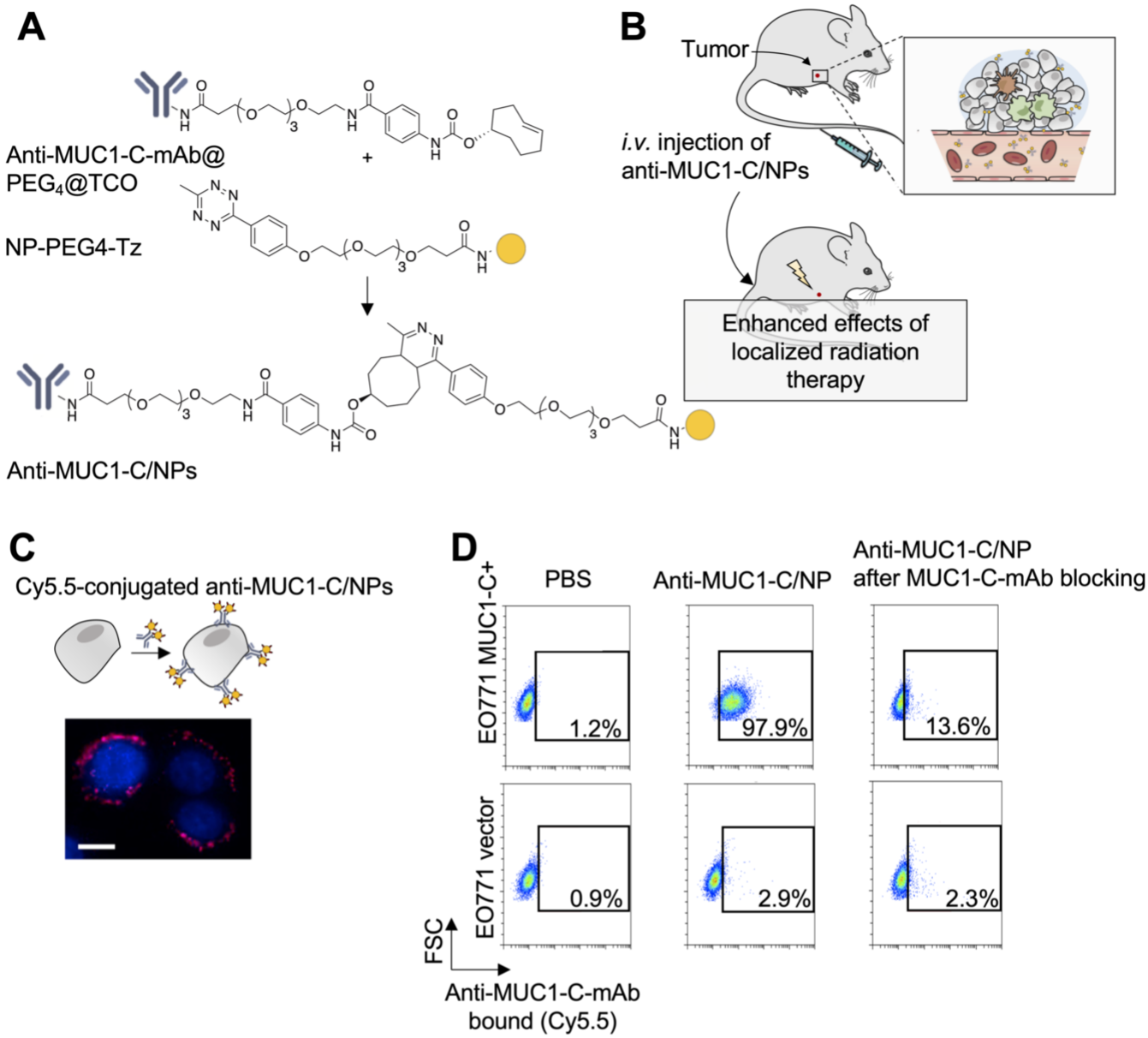
A
Anti-MUC1-C-mAb@
PEG4@TCO
+
NP-PEG4-Tz
Anti-MUC1-C/NPs
B
Tumor
i.v. injection of
anti-MUC1-C/NPs
Enhanced effects of
localized radiation
therapy
C
Cy5.5-conjugated anti-MUC1-C/NPs
D
PBS
Anti-MUC1-C/NP
Anti-MUC1-C/NP
after MUC1-C-mAb blocking
EO771 MUC1-C+
EO771 vector
1.2%
97.9%
13.6%
0.9%
2.9%
2.3%
FSC
Anti-MUC1-C-mAb
bound (Cy5.5)

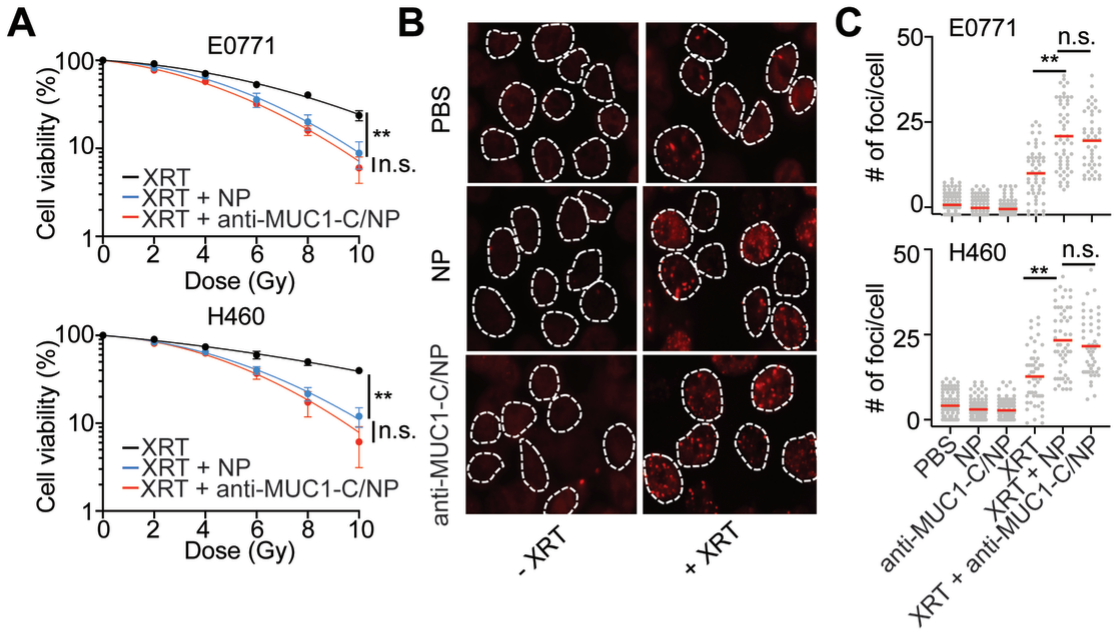
A
E0771
Cell viability (%)
100
10
1
0
2
4
6
8
10
Dose (Gy)
XRT
XRT + NP
XRT + anti-MUC1-C/NP
**
n.s.
H460
Cell viability (%)
100
10
1
0
2
4
6
8
10
Dose (Gy)
XRT
XRT + NP
XRT + anti-MUC1-C/NP
**
n.s.
B
PBS
NP
anti-MUC1-C/NP
- XRT
+ XRT
C
E0771
# of foci/cell
50
25
0
**
n.s.
H460
# of foci/cell
50
25
0
**
n.s.
PBS
NP
anti-MUC1-C/NP
XRT
XRT + NP
XRT + anti-MUC1-C/NP

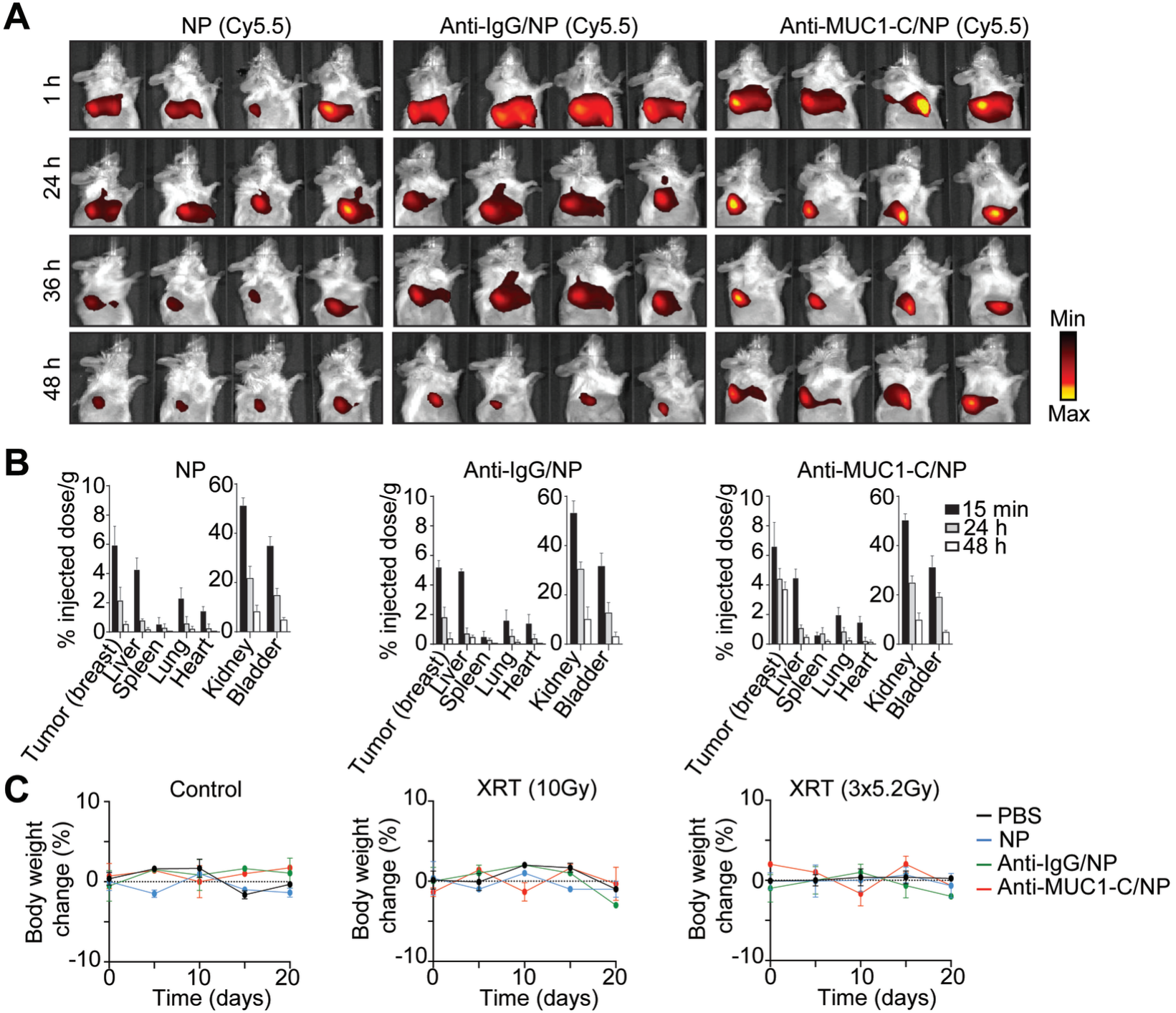
A
NP (Cy5.5)
Anti-IgG/NP (Cy5.5)
Anti-MUC1-C/NP (Cy5.5)
1 h
24 h
36 h
48 h
Min
Max
B
NP
Anti-IgG/NP
Anti-MUC1-C/NP
% injected dose/g
15 min
24 h
48 h
Tumor (breast)
Liver
Spleen
Lung
Heart
Kidney
Bladder
C
Control
XRT (10Gy)
XRT (3x5.2Gy)
Body weight change (%)
Time (days)
PBS
NP
Anti-IgG/NP
Anti-MUC1-C/NP

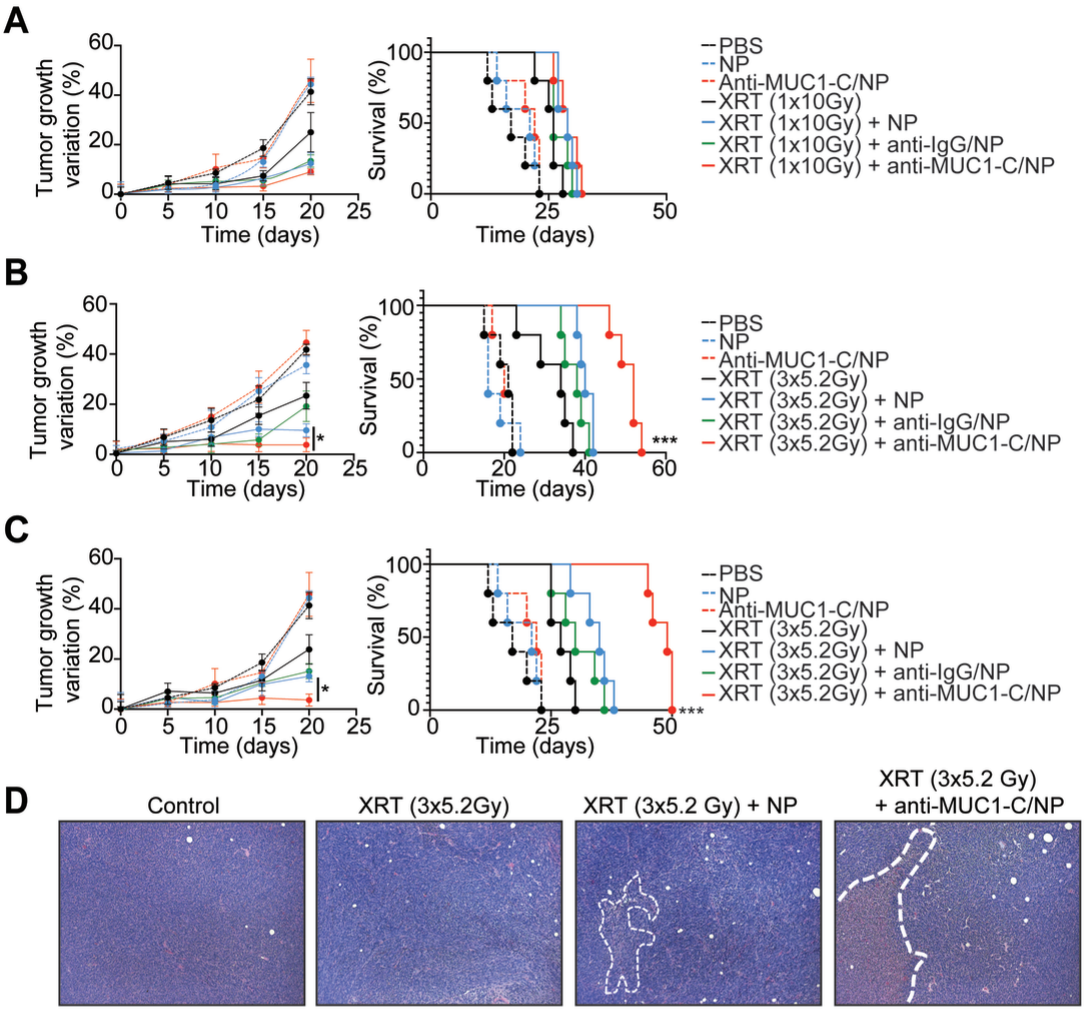
A
Tumor growth variation (%)
Time (days)
Survival (%)
Time (days)
PBS
NP
Anti-MUC1-C/NP
XRT (1x10Gy)
XRT (1x10Gy) + NP
XRT (1x10Gy) + anti-IgG/NP
XRT (1x10Gy) + anti-MUC1-C/NP
B
Tumor growth variation (%)
Time (days)
Survival (%)
Time (days)
*
***
PBS
NP
Anti-MUC1-C/NP
XRT (3x5.2Gy)
XRT (3x5.2Gy) + NP
XRT (3x5.2Gy) + anti-IgG/NP
XRT (3x5.2Gy) + anti-MUC1-C/NP
C
Tumor growth variation (%)
Time (days)
Survival (%)
Time (days)
*
***
PBS
NP
Anti-MUC1-C/NP
XRT (3x5.2Gy)
XRT (3x5.2Gy) + NP
XRT (3x5.2Gy) + anti-IgG/NP
XRT (3x5.2Gy) + anti-MUC1-C/NP
D
Control
XRT (3x5.2Gy)
XRT (3x5.2 Gy) + NP
XRT (3x5.2 Gy)
+ anti-MUC1-C/NP